mathematics

MDPI

Article

Analytical Solution for Bearing Capacity of Reinforced Strip Footings on Unsaturated Soils under Steady Flow

Xudong Kang and De Zhou *

School of Civil Engineering, Central South University, Changsha 410075, China; kangxudong@csu.edu.cn
* Correspondence: 210026@csu.edu.cn

Abstract: The study of analytical solutions for the bearing capacity of reinforced soil foundations is a very important topic in engineering mathematics. Existing evaluations of the foundation-bearing capacity on reinforced soils are based on dry conditions, while many foundations are located on unsaturated soils in real engineering. In this paper, a new formula for the bearing capacity of reinforced strip footings on unsaturated soils is presented. Two sliding failure mechanisms are constructed based on the position of the reinforcement layer relative to the sliding surface. The distribution of apparent cohesion in the depth direction is calculated by considering the effect of matrix suction. By additionally considering the work conducted by the reinforcement and the contribution of the apparent cohesion, the bearing capacity formula is obtained using the upper bound theorem of limit analysis. The bearing capacity solution is obtained by adopting the sequential quadratic programming (SQP) algorithm. Comparing the results under two failure mechanisms, the optimal bearing capacity and the optimal embedment depth of reinforcement are obtained. The results of this paper are consistent with those of the existing literature. Finally, the effects of reinforcement embedment depth, effective internal friction angle, uniform load, and unsaturated soil parameters on the optimal bearing capacity are investigated through parametric analysis. This paper provides useful recommendations for the engineering application of reinforced strip footings on unsaturated soils.

Keywords: reinforced soil foundations; unsaturated soils; steady flow; slide failure; upper bound

MSC: 49-06

Citation: Kang, X.; Zhou, D. Analytical Solution for Bearing Capacity of Reinforced Strip Footings on Unsaturated Soils under Steady Flow. *Mathematics* **2023**, *11*, 3746. https://doi.org/10.3390/math11173746

Academic Editors: Tuan A. Pham, Daniel Dias and Vasily Novozhilov

Received: 5 August 2023
Revised: 23 August 2023
Accepted: 29 August 2023
Published: 31 August 2023

1. Introduction

The bearing capacity of the foundation is one of the most critical indicators for assessing its performance. As reinforcement techniques have been widely used to enhance the bearing capacity of foundations on soft soils, the derivation of the bearing capacity solution for reinforced soil foundations has become a popular research topic in engineering mathematics. Existing studies on the above topic are based on dry soils or rocks [1–5]. However, many foundations are constructed on unsaturated soils in actual engineering [6,7]. Therefore, it is necessary to calculate the bearing capacity of reinforced foundations on unsaturated soils in order to provide recommendations for foundation design.

Research on the evaluation of the bearing capacity of foundations on reinforced soils is scarce, and most studies are based on traditional laboratory or field tests. Through experimental studies, Binquet and Lee [8] first demonstrated the significant enhancement in the bearing capacity of reinforced sand footings. Huang and Tatsuoka [9] predicted the variation of the bearing capacity of reinforced sand footings and analyzed the influence of material parameters and reinforcement arrangement. Subsequently, Das et al. [10] provided the optimal reinforcement parameters for saturated clays. Compared to the planar reinforced models, Raja and Shukla [11] pointed out that the wraparound reinforced model can lead to less foundation settlement and better stability. Some scholars have conducted

further experimental studies on the properties of reinforced soil foundations [12,13]. For reinforced soil foundations, the working modes of the reinforcement can be broadly categorized into the following three types: (a) Confinement effect: The frictional internal forces generated when the reinforcement and soil undergo relative sliding restrict the deformation of the soil, thereby increasing the bearing capacity of the foundation. Based on the kinematic approach of limit analysis and multi-block failure mechanisms, Michalowski [1] provided the variation of the bearing capacity of reinforced soil footings with the depth of reinforcement embedment. Manna et al. [2] considered a rigid pavement as an equivalent strip footing and assessed the effect of inclined ground on the bearing capacity of reinforced rigid pavements. Soufi et al. [3] constructed a new failure mechanism for reinforced soil foundations under seismic action and assessed the seismic bearing capacity of reinforced soil footings by adopting a pseudo-static approach. (b) Rigid boundary effect: The reinforcement is considered a rigid boundary for soil damage, suppressing the development of failure mechanisms in the deeper soil and thus enhancing the bearing capacity. Binquet and Lee [14] observed this phenomenon in experiments. Some researchers have also used this failure mode when evaluating the bearing capacity of footings on reinforced soils [1,2], considering both the above-mentioned failure modes and obtaining the optimal bearing capacity and corresponding optimal reinforcement burial by comparison. (c) Membrane effect: When the foundation is subjected to loading, the soil moves downward, causing deformation of the reinforcement. The deformed reinforcement generates a supportive force, thereby providing reinforcement. Kumar and Saran [15] proposed an empirical method for evaluating the bearing capacity of reinforced soil rectangular foundations according to this failure mode.

With the rapid development of numerical simulation techniques, some scholars have conducted finite element analyses on reinforced soil foundations [16–18]. Wang et al. [19] investigated the settlement of reinforced soil foundations using the discrete element method and visualized the load transfer as well as the spreading behavior of reinforced soil structures. Based on the three-dimensional discrete element method, Chen et al. [20] further investigated the intrinsic mechanisms, such as the deformation behavior and response of geogrids, and studied the influence of reinforcement parameters on foundation settlement. In addition, Nazeeh and Babu [21] used kriging surrogates to perform a reliability analysis of geogrid-reinforced soil foundations. In addition, some scholars have investigated the application of geotechnical seismic isolation (GSI) to different foundations, some of them using experimental studies [22] and others using finite element analyses [23,24].

However, it has been found that the existing studies on reinforced soil foundations are based on dry or saturated soils and have certain limitations. Shallow foundations in actual engineering are generally located on unsaturated soils, and the performance of footings largely depends on the shear strength of unsaturated soils. Therefore, it is crucial to consider the effects of unsaturated soil properties in the design of reinforced soil foundations. Such research can be applied in a variety of directions. For example, Bak et al. [25] studied the enhancement of foundation bearing capacity by using the Taguchi method, which can be extended to applications based on unsaturated soils using the ideas in this paper. It can also be used for foundations near slopes, for foundations on reinforced soil wall structures, and even for bridge abutment foundations. In addition, the seismic bearing capacity of reinforced foundations on unsaturated soils can be predicted by considering the seismic effect. This research topic is especially important for areas with frequent rainfall, so as to provide some theoretical reference for engineering practice.

Previous literature has shown that matric suction can significantly enhance the shear strength of unsaturated soils [26]. Compared to foundations on dry or saturated soils, foundations on unsaturated soils have greater bearing capacity because of the matric suction. When calculating the bearing capacity of footings on unsaturated soils, the modified Terzaghi's formula with the inclusion of matric suction is commonly used. Fredlund et al. [27] used two independent stress variables to linearly describe the relationship between the shear strength of unsaturated soils and matric suction. Oloo et al. [28] introduced the above

equation into Terzaghi's formula to assess the effect of matric suction on the pavement structure's performance. However, experimental studies have shown that there is a significant nonlinear connection between matric suction and bearing capacity that does not follow the assumed linear relationship [29–31]. Therefore, Lu and Likos [32] defined the suction stress, which consists of matric suction and some other physical and chemical forces, provided the distribution of suction stress with depth, and analyzed its change with factors such as different steady-state flows and temperature. Lu et al. [33] gave a new closed-form equation for the effective stress of unsaturated soils. Subsequently, many scholars have applied it to the analysis of foundation bearing capacity on unsaturated soils [34–36].

The description of effective stress using two independent variables (net stress and matric suction) has limitations, including difficulties in describing the changes in strength and suction and in smoothing the transition between saturated and unsaturated states. Lu et al. [33] used a single variable to represent effective stress, which also has some drawbacks, particularly in explaining the wetting process of unsaturated soils. However, Lu et al.'s equation has a wide range of applications, as it can be used for deformation analysis and shear strength analysis and can be combined with the limit analysis theorem.

In this paper, a new formula for calculating the bearing capacity solution of reinforced strip footings on unsaturated soils is proposed. Based on the different working modes of reinforcement, two multi-block failure mechanisms are constructed. The shear strength of soils at different depths was calculated using the effective stress equation proposed by Lu et al. Considering the effect of reinforcement and matric suction, the formulas for bearing capacity under the two multi-block failure mechanisms are derived using the upper bound theorem of limit analysis. The upper bound solution of the bearing capacity is obtained using a sequential quadratic programming (SQP) algorithm. Then, the results of the two failure mechanisms are compared for different depths of reinforcement embedment to obtain the optimal embedment depth of reinforcement and the corresponding optimal bearing capacity. Furthermore, the influences of different parameters on the optimal bearing capacity of reinforced foundations on unsaturated soils are analyzed.

2. Theoretical Framework

2.1. Upper Bound Theorem of Limit Analysis

The upper bound method can be used in a range of engineering problems [37–41], including tunnel stability, bearing capacity of foundations, slope stability, et al. The main idea of the theorem is summarized as follows: for a given kinematically admissible velocity field, the upper bound solution for the ultimate load can be obtained from the equality of the work performed by the internal force and the work performed by the external force, as shown in Equation (1). In this paper, the work conducted by the reinforcement is considered the work performed by the internal forces.

$$\int_S T_i v_i \mathrm{d}S + \int_V F_i v_i \mathrm{d}V = \int_V \sigma_{ij} \varepsilon_{ij} \mathrm{d}V \tag{1}$$

where T_i is the surface force, v_i is the velocity of the failure mechanism, F_i is the body force, S and V are the area and volume, respectively, σ_{ij} means the stress, and ε_{ij} means the corresponding plastic strain rate.

2.2. Slide Failure Mode

2.2.1. Symmetric Multi-Block Failure Mechanism

According to previous research [1], it is feasible to research the failure mode of reinforced soil footings by using the mechanism properties of unreinforced soil. When the traditional Prandtl failure mechanism is used, the integral calculation of the work performed by the reinforcement will be very complicated and inefficient, so the symmetric multi-block failure mechanism is used. Depending on the relative positions of the reinforcement and the slide surface, two multi-block failure mechanisms are constructed, as demonstrated in Figures 1 and 2. The velocity field of the failure mechanism is shown in

Figure 3. In Figure 1, the right half of the failure mechanism is divided into n pieces of rigid bodies, except for the ABC rigid body. Therefore, the geometry of the mechanism is determined by $2n + 1$ variables (θ, α_i, β_i). Eccentricity and inclination of loads are not considered in this paper, and it is assumed that only vertically concentric loads act on the foundation.

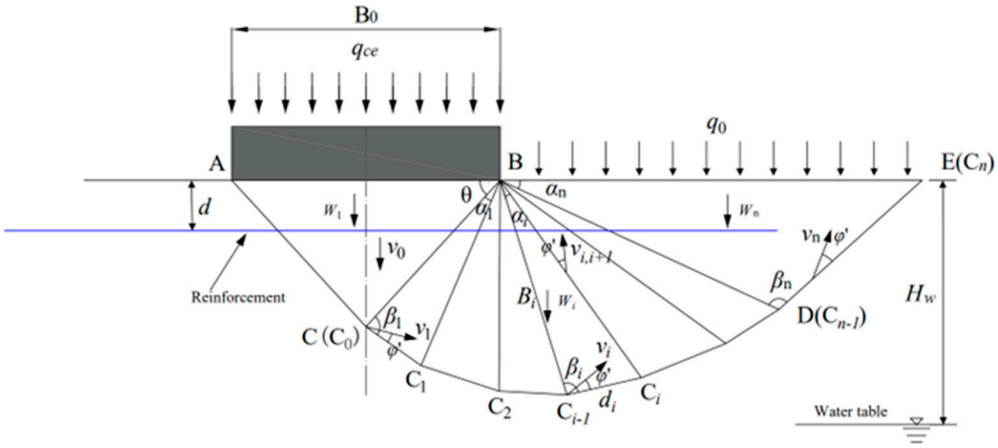

Figure 1. The geometry and force schematic of the shallow sliding failure mechanism (M1).

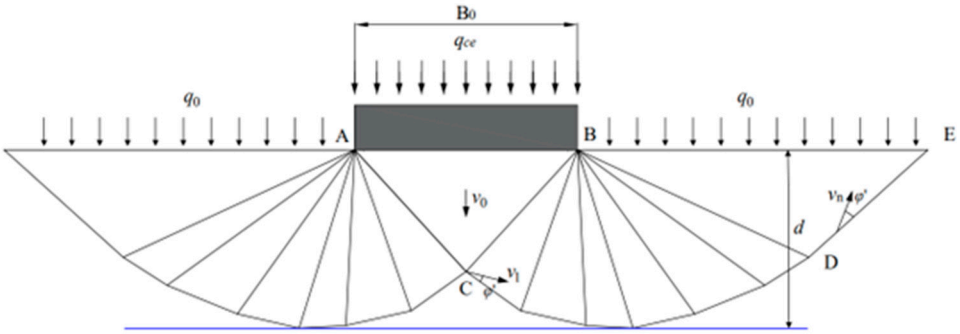

Figure 2. The geometry and forces schematic of M2.

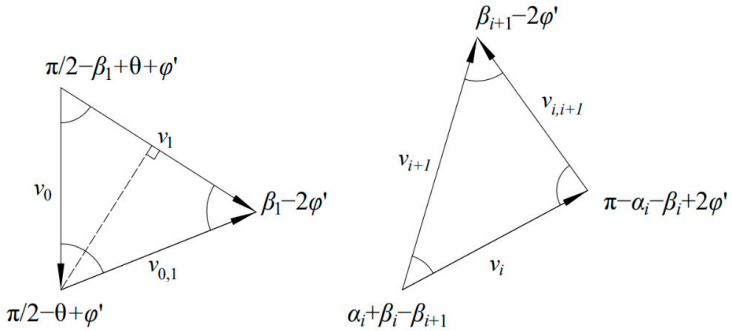

Figure 3. Velocity vector diagram.

The width of the foundation is B_0 and the other geometrical dimensions of the mechanism, as well as the magnitude of the velocity vector, can be derived as follows:

$$B_i = \frac{B_0}{2\cos\theta}\prod_{j=1}^{i-1}\frac{\sin\beta_j}{\sin(\alpha_j+\beta_j)} \tag{2}$$

$$d_i = \frac{B_0}{2\cos\theta}\frac{\sin\alpha_i}{\sin(\alpha_i+\beta_i)}\prod_{j=1}^{i-1}\frac{\sin\beta_j}{\sin(\alpha_j+\beta_j)} \tag{3}$$

$$v_1 = v_0 \frac{\sin\left(\frac{\pi}{2} - \theta + \varphi'\right)}{\sin(\beta_1 - 2\varphi')} \tag{4}$$

$$v_{i+1} = v_i \frac{\sin(\pi - \alpha_i - \beta_i + 2\varphi')}{\sin(\beta_{i+1} - 2\varphi')} \tag{5}$$

$$v_{i,i+1} = v_i \frac{\sin(\alpha_i + \beta_i - \beta_{i+1})}{\sin(\beta_{i+1} - 2\varphi')} \tag{6}$$

where v_0 is the velocity of the ABC rigid body, B_i is the length of the velocity discontinuity line, d_i is the length of the slide surface of each rigid body, v_i is the velocity of the ith block, and $v_{i,i+1}$ is the velocity on the velocity discontinuity line.

A key factor in the study of the bearing capacity of footings on reinforced soils is the identification of the critical failure mechanism. The foundation bearing capacity gradually increases as the embedment depth of reinforcement increases; however, previous experimental studies [14] have shown that when the reinforcement embedment depth increases in a certain level, the whole mechanism develops above the reinforcement (Figure 2). Therefore, two multi-block failure mechanisms, M1 and M2, are used in this paper. The optimal depth of the reinforcement as well as the optimal bearing capacity are obtained by comparing the results of the bearing capacity under the above two mechanisms.

2.2.2. Work Dissipation Rate of the Reinforcement

The rate of dissipation of internal work per unit width of reinforcement when the reinforcement slides relative to soils is expressed as follows:

$$D = 2l_e(\mu\sigma_n + c_{\text{int}})v_h \tag{7}$$

$$\mu = f_b \tan\varphi \tag{8}$$

$$c_{\text{int}} = f_c c \tag{9}$$

where v_h means the relative velocity of reinforcement and soil, μ means the friction coefficient of the reinforcement-soil contact interface, σ_n means the normal stress on reinforcement, l_e means the effective length of reinforcement, c_{int} means the interface shear strength, and both f_b and f_c mean bond coefficients. According to a previous study [1], both f_b and f_c are taken as 0.6.

The key factor in calculating the work dissipation rate of the reinforcement is the determination of σ_n. Since the true magnitude of σ_n is undetectable, a piece-wise linear distribution of σ_n is used in this paper as suggested in previous literature [1], as shown in Figure 4. The stresses on reinforcement below the foundation are calculated by means of an overall force balance in the vertical direction. The angle δ is indeterminate and takes values from 0 to $\frac{\pi}{4} + \frac{\varphi}{2}$. The distribution of σ_n is influenced by the magnitude of δ. According to Huang and Tatsuoka [9], a "deep footing effect" occurs when $d/B_0 = 1$, in which case $\delta = 0$. As the reinforcement gets longer, the angle δ increases. Since the real distribution of σ_n is unknown, the analysis in this paper adopts the conservative assumption that $\delta = 0$. The stress distribution is shown in Figure 5.

The σ_n on reinforcement is divided into three segments, HK segment: $\sigma_n = \gamma d + q_{ce}$, FG segment: $\sigma_n = \gamma d + q_0$, and the normal stress value in the middle part is taken as a linear interpolation with the following expression:

$$\sigma_{n,i} = \gamma d + q_{ce}\left(1 - \frac{\sum_{1}^{i-1} l_{e,i} + \sum_{1}^{i} l_{e,i}}{2d\cot(\theta)}\right) + q_0\left(\frac{\sum_{1}^{i-1} l_{e,i} + \sum_{1}^{i} l_{e,i}}{2d\cot(\theta)}\right) \qquad 1 \le i \le k-1 \tag{10}$$

$$\sigma_{n,i} = \gamma d + q_{ce}\left(\frac{\left(d\cot(\theta) - \sum_{1}^{k-1} l_{e,i}\right)^2}{2d\cot(\theta) l_{e,k}}\right) + q_0\left(1 - \frac{\left(d\cot(\theta) - \sum_{1}^{k-1} l_{e,i}\right)^2}{2d\cot(\theta) l_{e,k}}\right) \qquad i = k \tag{11}$$

where d is the reinforcement embedment depth, i is the number of the block, k is the number of the block through which the vertical line through point A (B) passes, and $l_{e,i}$ is the effective length of reinforcement through the ith block. The detailed formulas for $l_{e,i}$ are shown in the Appendix A.

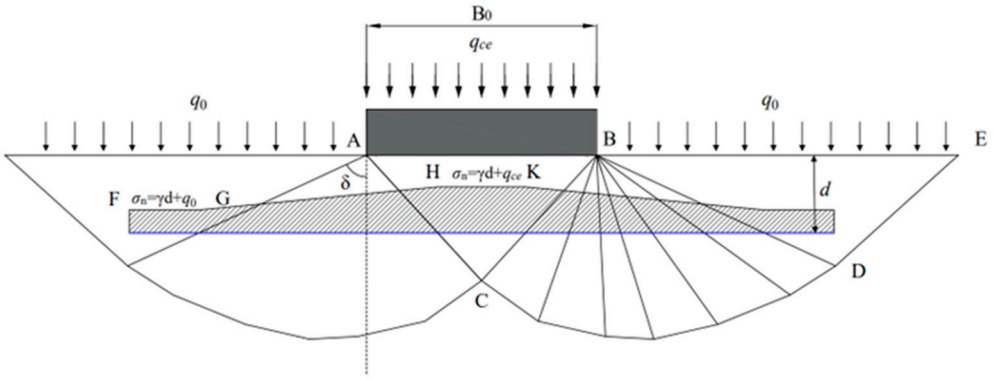

Figure 4. Stress diagram for M1.

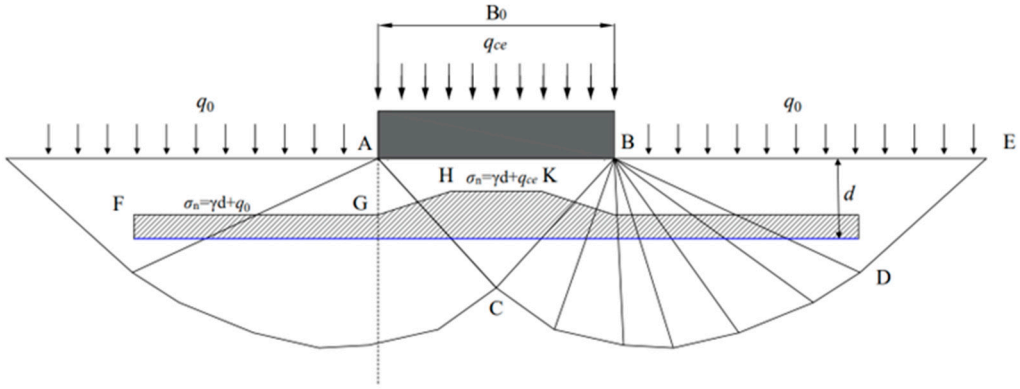

Figure 5. Stress diagram for M1 used in this paper.

2.3. Properties of Unsaturated Soils

The assessment of effective stress is crucial to the research of unsaturated soil properties. Based on previous research [27], Lu and Likos [32] proposed a unified method to characterize the effective stress, which is described as Equation (12).

$$\sigma' = \sigma - u_a - \sigma^s \tag{12}$$

where σ means the total stress, σ^s means the suction stress, σ' means the effective stress, and u_a means the pore air pressure. A positive value of σ' represents compressive stress. To characterize the magnitude of the σ^s, Lu et al. [33] give an equation for its closed solution, which can be described as follows:

$$\sigma^s = -(u_a - u_w) \qquad (u_a - u_w) \leq 0 \tag{13}$$

$$\sigma^s = -\frac{(u_a - u_w)}{\left\{1 + [\alpha(u_a - u_w)]^{\psi}\right\}^{(\psi-1)/\psi}} \qquad (u_a - u_w) > 0 \tag{14}$$

where $u_a - u_w$ means the matric suction, u_w means the pore water pressure, and α and ψ are the fitting coefficients of soils. In unsaturated soils, the pore air pressure is not equal

to the pore water pressure; the shrinkage film (water-air interface) is subjected to an air pressure that is greater than the water pressure, and this pressure difference is known as matrix suction. When $(u_a - u_w) \leq 0$, it means that the soil is saturated; on the contrary, the soil is unsaturated. In addition, there is a range of values for α and ψ. α is taken from 0 to 0.5 and ψ takes values between 1.1 and 8.5.

In this paper, a model of Gardner [42] and Darcy's law is adopted to characterize the matrix suction, assuming that $(u_a - u_w) = 0$ at $z = 0$, the formulas for matric suction are as follows:

$$k = k_s e^{\alpha(u_a - u_w)} \tag{15}$$

$$u_a - u_w = -\frac{1}{\alpha} \ln\left[\left(1 + \frac{q}{k_s}\right) e^{-\gamma_w \alpha z} - \frac{q}{k_s}\right] \tag{16}$$

where k_s and k mean the hydraulic conductivity of saturated and unsaturated soils, respectively, γ_w means unit weight of water (10 kN/m^3), q means the flow rate, and z means height above the water table. $q > 0$ indicates infiltration, $q < 0$ indicates evaporation, and $q = 0$ indicates no-flow. Bringing Equation (16) into Equation (14) yields an expression for the suction stress σ^s as follows:

$$\sigma^s = \frac{1}{\alpha} \frac{\ln\left[\left(1 + \frac{q}{k_s}\right) e^{-\gamma_w \alpha z} - \frac{q}{k_s}\right]}{\left(1 + \left\{-\ln\left[\left(1 + \frac{q}{k_s}\right) e^{-\gamma_w \alpha z} - \frac{q}{k_s}\right]\right\}^{\psi}\right)^{(\psi-1)/\psi}} \tag{17}$$

The cohesion contributed by the suction stress is known as the apparent cohesion, which is expressed as follows:

$$c_{app} = -\sigma^s \tan \varphi' \tag{18}$$

Bringing Equation (17) into Equation (18) yields the final expression for c_{app}. The total cohesion c of the soil can be viewed as consisting of c' and c_{app} as follows:

$$c = c' + c_{app} \tag{19}$$

3. Materials and Methods

3.1. Selection of Materials

In order to obtain generally applicable conclusions, with reference to Du et al. [35] and Xu and Zhou [36], four representative unsaturated soils were selected in this paper, and the values of relevant parameters were taken as shown in Table 1. Besides three values of q were assigned, $q = -3.14 \times 10^{-8}$ means evaporation, $q = 0$ means no-flow, and $q = 1.15 \times 10^{-8}$ means infiltration.

For the reinforcement material, this paper assumes that the reinforcement is strong enough and that the power due to reinforcement extension is neglected. The reinforcement is arranged horizontally and symmetrically based on the center of the foundation. Based on previous experience [1], the total length of the reinforcement is taken as $4B_0$. In addition, the default values for the other parameters are used unless noted otherwise, i.e., $B_0 = 1$ m, $\varphi' = 30^\circ$, $q_0 = 0$ kPa, $q = 0$ m/s, and $H_w = 4B_0$.

Table 1. Material parameters for four soil types.

Soil Types	α (kPa^{-1})	ψ	k_s (m/s)	c' (kPa)	γ (kN/m^3)
Clay	0.005	2	5×10^{-8}	10	18
Silt	0.01	2	5×10^{-7}	10	18
Loess	0.025	4	5×10^{-6}	0	18
Sand	0.1	4	5×10^{-5}	0	18

3.2. The Upper Bound Method

3.2.1. Calculation of Internal Power

The internal power of the entire failure mechanism is composed of three parts: the power D_1 of the effective cohesive, the power D_2 of the apparent cohesive, and the power D_3 of the reinforcement contributed by the effective cohesive. The total internal power is expressed as follows:

$$D_{\text{int}} = 2(D_1 + D_2 + D_3) \tag{20}$$

The distribution of the effective stress c' along the vertical direction is constant, so it can be calculated in the traditional way of internal power calculation. Taking the right half of the symmetric mechanism as an example, it consists of three components: the power along the BC line, the power along the B_i, and the power along the sliding surface d_i. The sum of the three is expressed as follows:

$$D_1 = c' B_0 v_0 (f_1 + f_2 + f_3) \tag{21}$$

where f_1, f_2 and f_3 are all described in detail in Appendix A, and v_0 is the velocity of block ABC. Since the distribution of apparent cohesion c_{app} along the vertical direction is nonlinear, the calculation of the power contributed by it requires integration, expressed as follows:

$$D_2 = \sum_{i=1}^{n} \int_0^{B_i \sin \sum_{j=1}^{i-1} (\theta + \alpha_j)} \frac{c_{app} v_{i-1,i} \cos \varphi'}{\sin \sum_{j=1}^{i-1} (\theta + \alpha_j)} \, \mathrm{d}y + \frac{1}{2} \sum_{i=1}^{n} \left(\sigma^s_{C_{i-1}} + \sigma^s_{C_i} \right) d_i v_i \sin \varphi' \tag{22}$$

where $\sigma^s_{C_{i-1}}$ and $\sigma^s_{C_i}$ mean the suction stress of points C_{i-1} and C_i, respectively. The values of the above two parameters can be calculated by Equation (17). Since the properties of the reinforcement-soil interface are unknown, the internal power of the reinforcement that may be contributed by the apparent cohesion is neglected in this paper.

$$D_3 = 2 \sum_{i=1}^{n} f_c l_{e,i} c' v_i \cos \theta_i \tag{23}$$

$$\theta_i = \beta_i - \varphi' - \theta - \sum_{1}^{i-1} \alpha_i \tag{24}$$

where θ_i means the angle between the velocity of the ith block and the horizontal line.

3.2.2. Calculation of External Power

The power of external forces consists of the power W_1 of the foundation load, the power of W_2 the self-weight of the soil, the power W_3 of the uniform load, and the power W_4 contributed by the reinforcement. The total external power is expressed as follows:

$$W_{ext} = W_1 + W_2 + W_3 + 2W_4 \tag{25}$$

The power of the foundation load is expressed as follows:

$$W_1 = q_{ce} B_0 v_0 \tag{26}$$

The power of the self-weight of the soil is expressed as follows:

$$W_2 = 0.5 \gamma {B_0}^2 v_0 (f_4 + f_5) \tag{27}$$

where γ means the unit weight of soils. The power of the uniform load is expressed as follows:

$$W_3 = q_0 B_0 v_0 f_6 \tag{28}$$

where f_4, f_5 and f_6 are all described in detail in the Appendix A. According to Equation (7), the external power contributed by the reinforcement is expressed as follows:

$$W_4 = 2\sum_{i=1}^{n} \mu l_{e,i}\sigma_{n,i}v_i \cos\theta_i \tag{29}$$

3.2.3. Formula of Bearing Capacity

Bringing the above internal and external powers into Equation (30) yields an expression for the bearing capacity q_{ce}. Since the effect of apparent cohesion is considered in this paper, the bearing capacity formula cannot be written in a superposition form such as the classical Terzaghi's formula but can be expressed as a function containing $2n + 1$ variables as follows:

$$q_{ce} = f(\alpha_i, \beta_i, \theta) \qquad (i = 1, 2, 3 \cdots n) \tag{30}$$

Combined with the constraints given in Appendix A, the above function is optimized using a sequential quadratic programming (SQP) algorithm to obtain an analytical solution for the bearing capacity. In order to make the structure of this paper clearer, the flowchart of this study is given in Figure 6.

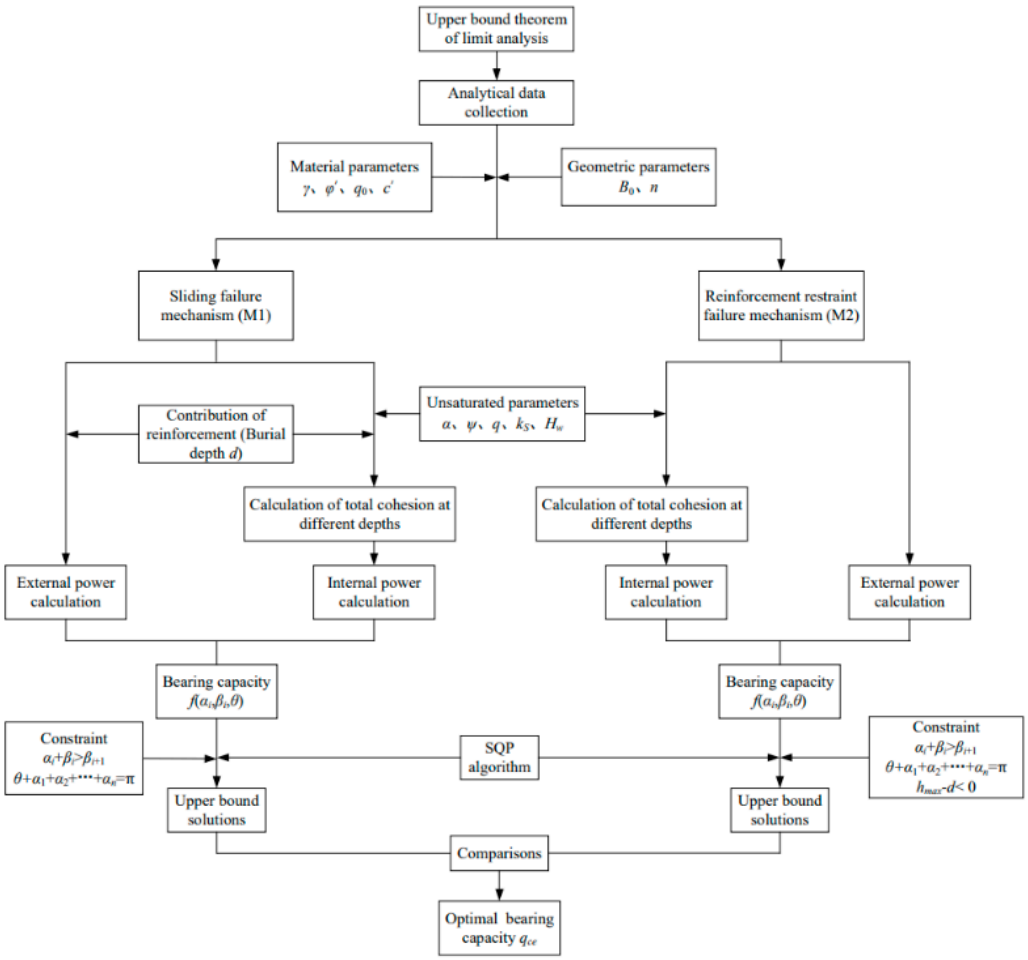

Figure 6. Flowchart of the research in this paper.

4. Validation of Results

Based on the upper bound theorem, an analytical solution formula is given for the bearing capacity of geotechnical reinforced footings on unsaturated soils. The purpose of this section is to verify the validity of the results obtained from the above formula.

4.1. Comparison for Dry Soils without Reinforcement

The first step in optimizing the bearing capacity function is to choose the right number n of rigid bodies for the failure mechanism. In general, the more the failure mechanism is divided into blocks, the more accurate the calculations will be. However, considering the error as well as the efficiency of the calculation, this paper takes $n = 15$. For the case where reinforcement as well as seepage are not considered, it takes $\varphi = 40^\circ$ and Table 2 demonstrates the change of the bearing capacity coefficient N_γ with n. As can be seen in Table 2, there is only a 0.13% decrease in the results for $n = 15$ compared to the results for $n = 14$. As n continues to increase, the change becomes even smaller and essentially negligible.

Table 2. N_γ varies with the number of blocks n for $\varphi = 40^\circ$.

n	N_γ	Reduction (%)
5	543.726	
6	171.674	68.43
7	128.795	24.98
8	122.934	4.55
9	121.572	1.11
10	120.993	0.48
11	120.580	0.34
12	120.270	0.26
13	120.032	0.20
14	119.844	0.16
15	119.694	0.13

In addition, the bearing capacity coefficients were compared with those of Soubra [43], as shown in Table 3. The results of this paper are very close to those of Soubra [43]. Therefore, it is confirmed that the value of n chosen in this paper is reliable.

Table 3. Comparisons of bearing capacity coefficients.

$\varphi(^\circ)$	N_γ		N_q		N_c	
	Soubra (1999) [42]	This Paper	Soubra (1999) [42]	This Paper	Soubra (1999) [42]	This Paper
0	-		1.00	1.00	5.15	5.42
5	-		1.57	1.59	6.50	6.70
10	-		2.47	2.50	8.36	8.53
15	1.95	1.94	3.95	3.98	10.99	11.12
20	4.49	4.48	6.41	6.43	14.86	14.93
25	9.81	9.80	10.69	10.69	20.77	20.77
30	21.51	21.49	18.46	18.44	30.24	30.22
35	49.00	48.96	33.44	33.40	46.33	46.28
40	119.84	119.69	64.58	64.48	75.77	75.65
45	326.59	326.05	135.99	135.70	134.99	134.70
50	1042.48	1040.07	322.88	321.90	270.09	269.26

4.2. Comparison for Dry Soils Considering Reinforcement

To verify the validity of the calculations of reinforcement power in this paper, the results of the bearing capacity of the foundation on dry soils are compared with those of other literature [1,3,44], as shown in Figure 7. The results of this paper have a similar trend to those of other literature, i.e., the bearing capacity ratio increases and then decreases with the increase in the embedment depth of reinforcement. The reinforcement embedment depth corresponding to the peak of the curve is the optimal embedment depth. Therefore, the optimal embedment depth is obtained by finding the location where the bearing capacity is the same under both failure mechanisms, and the optimal bearing capacity can be obtained by corresponding to the optimal embedment depth. The rising part of the curve corresponds to M1, and the falling part of the curve corresponds to M2.

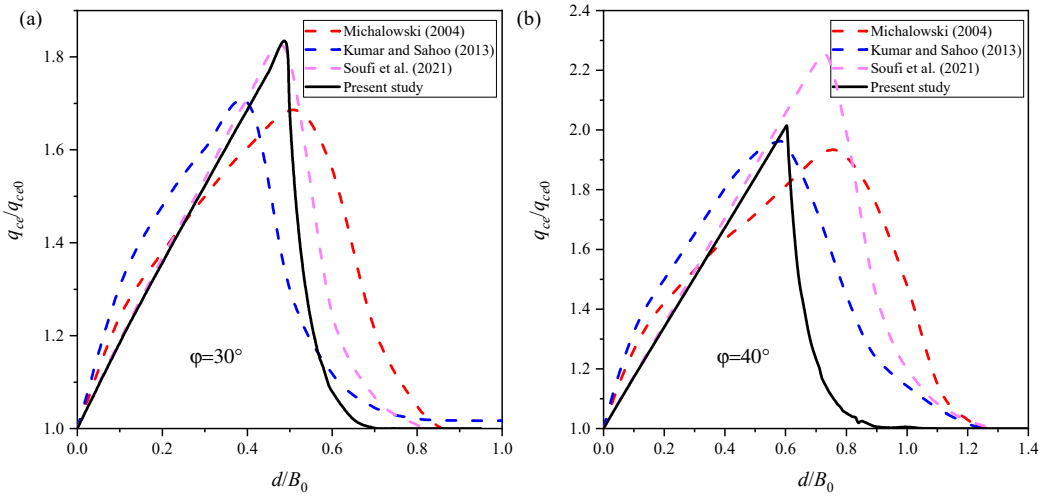

Figure 7. Comparisons of bearing capacity ratios for dry soils compared to the unreinforced case ($q_0 = c = 0$). (**a**) $\varphi = 30°$, (**b**) $\varphi = 40°$ [1,3,15].

From Figure 7, the curves do not match exactly, which is due to the use of different analysis methods as well as optimization algorithms. However, the optimal reinforcement embedment depth as well as the bearing capacity ratios are within a certain range. It confirms the accuracy of the reinforcement power calculations in this paper. In the subsequent analysis, if not specified, the foundation bearing capacity provided in this paper is the optimal bearing capacity at the optimal embedment depth of the reinforcement.

4.3. Comparison for Unsaturated Soils

Figure 8 illustrates a comparison of the bearing capacity values of the foundation on unsaturated soils with other literature [34–36], and the values of the parameters are $B_0 = 1$ m, $\varphi' = 20°$, $q_0 = 0$ kPa, $q = 0$ m/s, $\psi = 1.8$, $k_s = 5 \times 10^{-8}$ m/s, and $\alpha = 0.005$ kPa^{-1}. The bearing capacities all show an increasing trend with increasing H_w/B_0, and the results of this paper are very similar to those of Xu and Zhou [36] and smaller than those of two other studies. When $H_w/B_0 = 10$, the results of this paper are about 43% smaller than those of Vahedifard and Robinson [34] and about 15.5% smaller than those of Du et al. [35]. Differences in the results are due to differences in the analytical methods and in the selection of the failure mechanism. Thus, the comparisons in the above subsections prove that the analytical method of this paper is reliable and the results are precise.

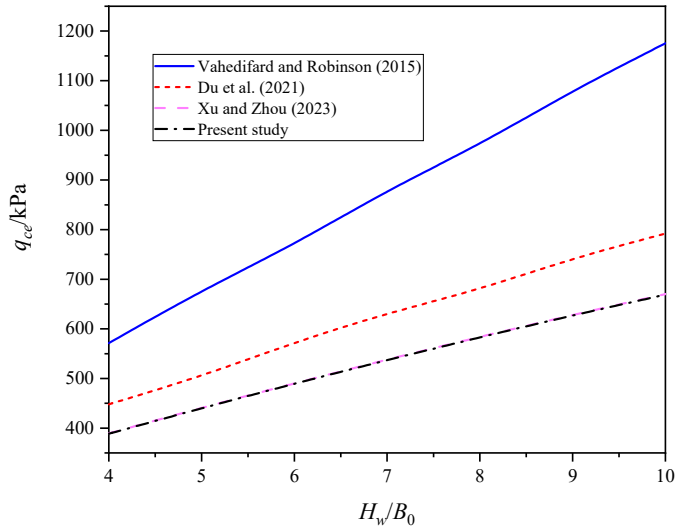

Figure 8. Comparison of the bearing capacity of the unsaturated soil foundation [34–36].

5. Parametric Analysis and Discussion

To deeply investigate the influence of reinforcement embedment depth and unsaturated soil properties on the bearing capacity of strip footings, the relevant parameters are analyzed in this section.

5.1. Effect of d/B_0

For the reinforced soil foundation, the most important factor is the embedment depth of reinforcement, so how to find the corresponding embedment depth of reinforcement when the bearing capacity is maximized is the focus of this study. As Figure 7 shows the variation of the q_{ce}/q_{ce0} of the foundation on dry soils with d/B_0, the optimal embedment depth is determined by comparing the bearing capacity under both failure mechanisms. In addition, it can be found that the optimal embedment depth is different at $\varphi = 30°$ and $\varphi = 40°$.

Figure 9 illustrates that for four different unsaturated soils, the change of the q_{ce}/q_{ce0} of strip footings with d/B_0 at different flow rates q. For four unsaturated soils, the optimal d/B_0 are all in the range of 0.49–0.56, which is essentially no difference. For the clay, the optimal d/B_0 increases as the flow rate q increases. However, for the other three types of soil, q does not affect the value of the optimal d/B_0. Although the optimal d/B_0 is similar for the four soils, the bearing capacity ratios q_{ce}/q_{ce0} are different, i.e., the enhancing effect of reinforcement on the q_{ce} is different. For the sand, the reinforcement effect is the most obvious, with a bearing capacity ratio q_{ce}/q_{ce0} close to 1.8 when the reinforcement is at the optimal d/B_0. The reason for the above result may be that the q_{ce} of foundations on sand are inherently low.

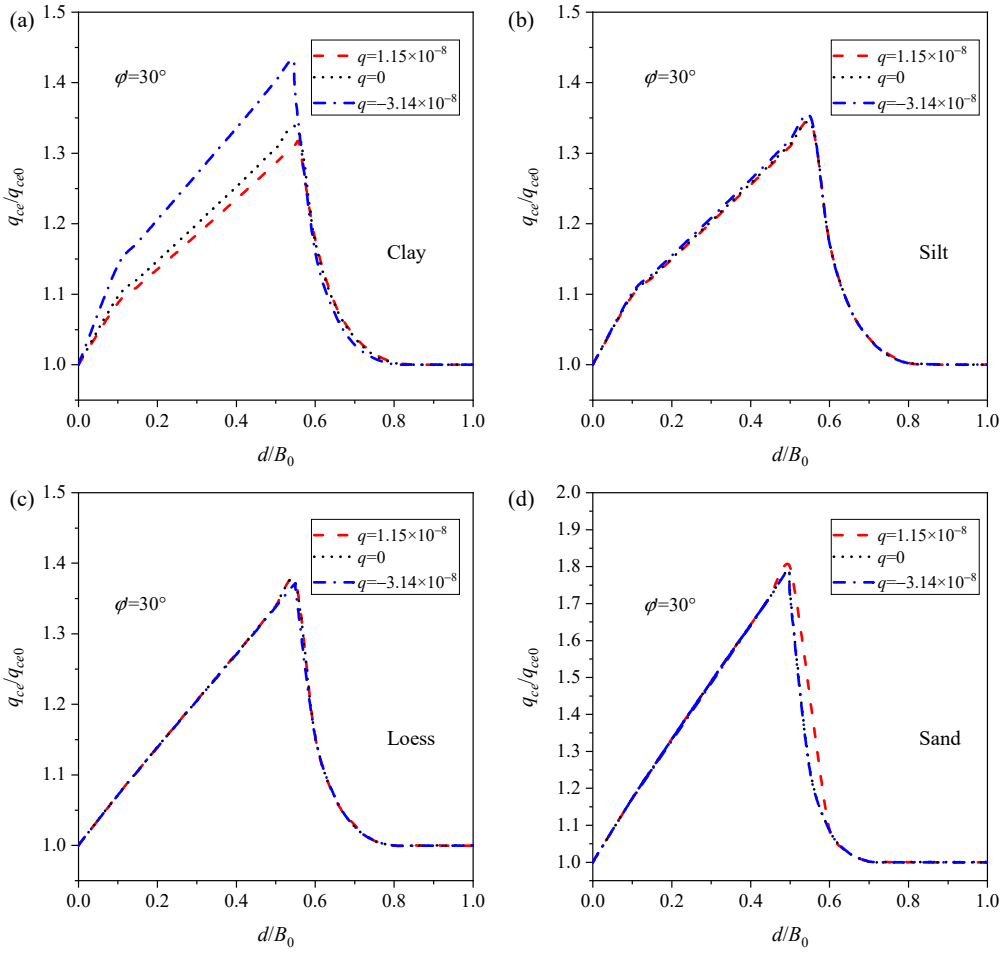

Figure 9. The bearing capacity ratio q_{ce}/q_{ce0} varies with d/B_0 at different q. (**a**) Clay, (**b**) Silt, (**c**) Loess, (**d**) Sand.

Figure 10 illustrates that for the clay, the change in the bearing capacity ratio q_{ce}/q_{ce0} of foundations with d/B_0 at different effective internal friction angle φ'. In each case of φ', the trend of q_{ce}/q_{ce0} with d/B_0 is the same, i.e., it increases and then decreases. However, it can be found that both q_{ce}/q_{ce0} and d/B_0 increase as φ' increases. When $\varphi' = 40°$, the optimal reinforcement embedment depth is equal to $0.648B_0$ and the optimal bearing capacity is equal to $1.467q_{ce0}$. Combining the above analyses, the effective angle of internal friction has an important effect on both the optimal embedment depth and the optimal bearing capacity ratio, while the type of soil, or effective cohesion, has a greater influence on the optimal bearing capacity ratio and a smaller effect on the optimal embedment depth. Therefore, the most important factor for evaluating the bearing capacity of reinforced soil footings is the selection of the effective angle of internal friction of the soil, while for the reinforced foundation on unsaturated clay, the flow rate q also has a certain influence.

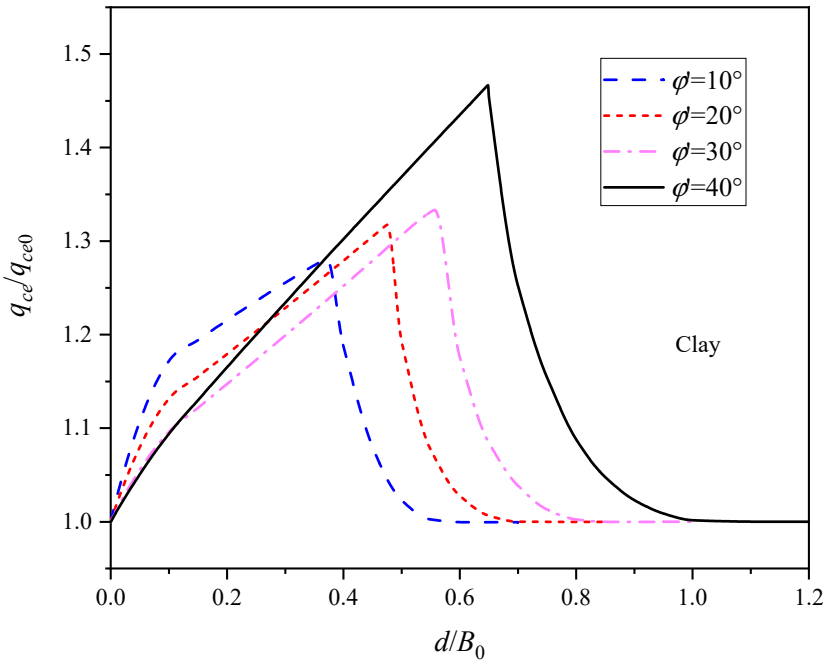

Figure 10. The bearing capacity ratio q_{ce}/q_{ce0} varies with d/B_0 at different φ' for the clay.

By regression analysis of the obtained results, the formulas for the bearing capacity of four typical unsaturated soils were obtained, as shown in Figure 11. It can be seen from Figure 11 that these curves fit well with the obtained results and can predict the bearing capacity of foundations at different burial depths of the reinforcement. The above expressions are simple in form and easy to apply, and they can provide some benefit to engineering practice. However, for a detailed analysis, it is also necessary to use Equation (30).

Based on the actual optimization results, Figure 12 depicts the critical failure surfaces for four soils under the reinforced and unreinforced cases, respectively, with default parameters. Compared to the unreinforced case, the failure mechanism of the foundation on reinforced soils continues to develop downwardly, so the bearing capacity is improved. For the unsaturated sand, the q_{ce} of the unreinforced foundation is 211.56 kPa, which is the smallest compared to the other three unsaturated soils, so its bearing capacity ratio after reinforcement is the largest, and it also shows that for the foundation on unsaturated sand, the reinforcement effect is the most significant. In addition, the greater the extent of the failure mechanism, the greater the bearing capacity. This is the essential reason why reinforcement measures can increase the bearing capacity of foundations.

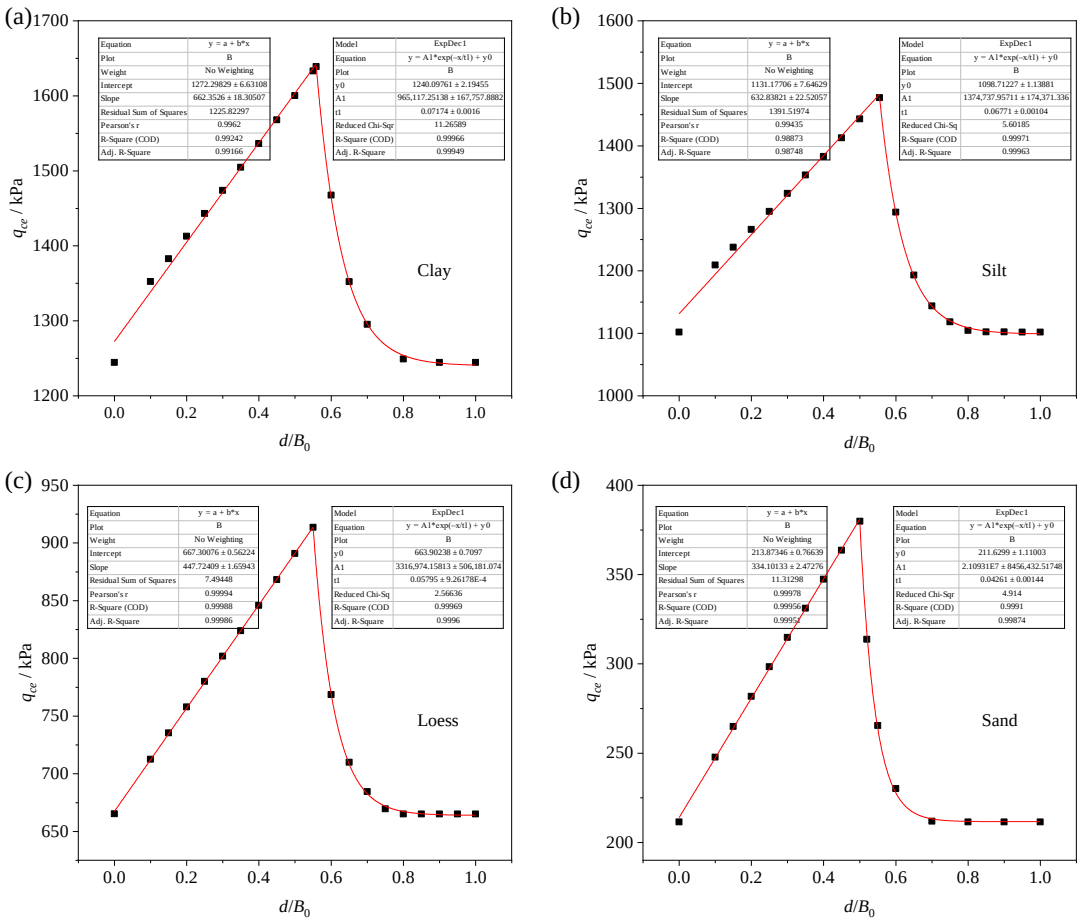

Figure 11. Fitted curves of the bearing capacity for four unsaturated soils. (**a**) Clay, (**b**) Silt, (**c**) Loess, (**d**) Sand.

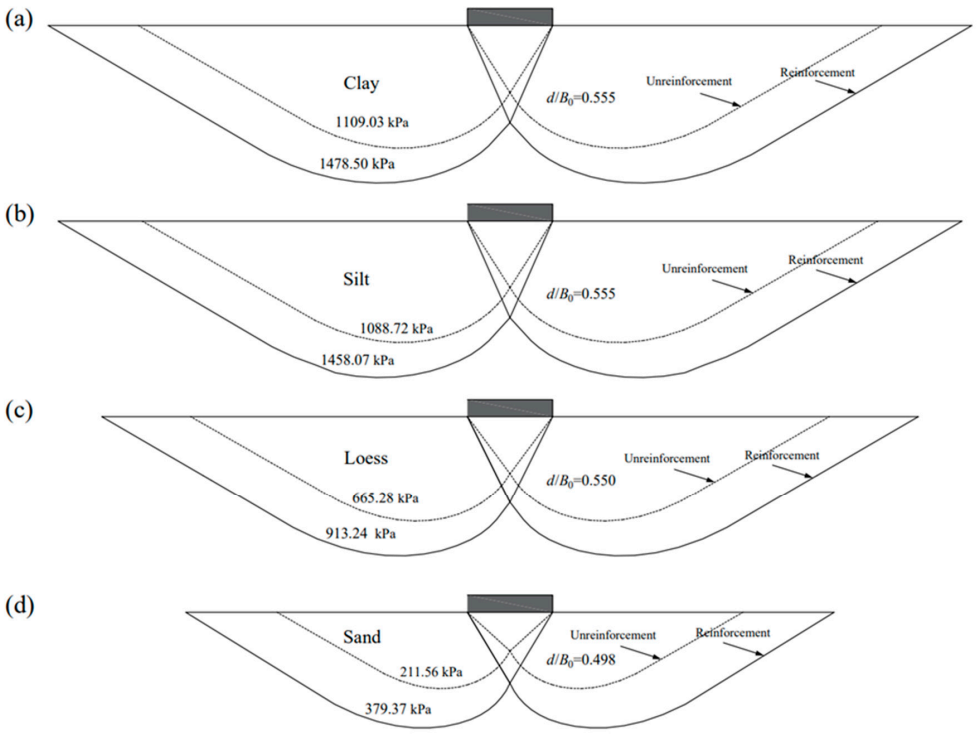

Figure 12. Critical failure surfaces for the four soils. (**a**) Clay, (**b**) Silt, (**c**) Loess, (**d**) Sand.

In order to facilitate the application to engineering practice, Figure 13 gives the range of embedment depths corresponding to 50% of the maximum increase of q_{ce} for the four types of soils at the default values of the parameters. In addition, the variation of d/B_0 with φ' is shown, again confirming the above discussion. The optimal embedment depth curves are all closer to the upper boundary because the curve (Figure 9) of the change in q_{ce}/q_{ce0} with d/B_0 decreases rapidly in the second half of the curve, and therefore the reinforcement must not be embedded too deep, or the failure mechanism will develop above the reinforcement.

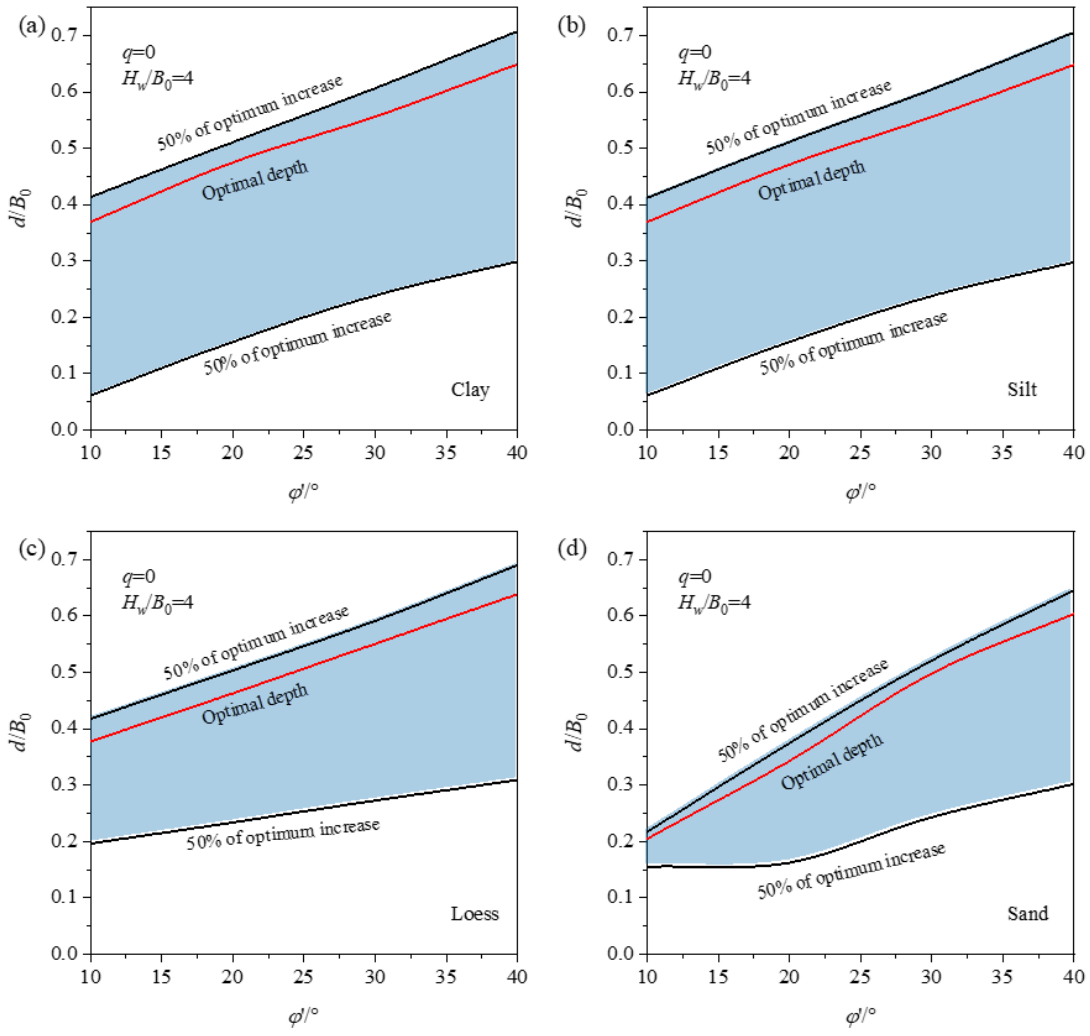

Figure 13. Variation of optimal embedment depth and embedment depth at a maximum 50% increase in bearing capacity with φ'. (**a**) Clay, (**b**) Silt, (**c**) Loess, (**d**) Sand.

5.2. Effect of φ' and q_0

In this paper, the effect of effective internal friction angle on the optimal bearing capacity of reinforced footings on unsaturated soils is investigated, as shown in Figure 14. For the four unsaturated soils, the optimal bearing capacity q_{ce} follows the same trend, increasing with φ'. After φ' is greater than 30°, the rate of increase of the q_{ce} becomes faster. Therefore, the effective angle of internal friction φ' is an important parameter, both for the optimal embedment depth and for the optimal bearing capacity. At the same time, the analysis of the previous section is confirmed.

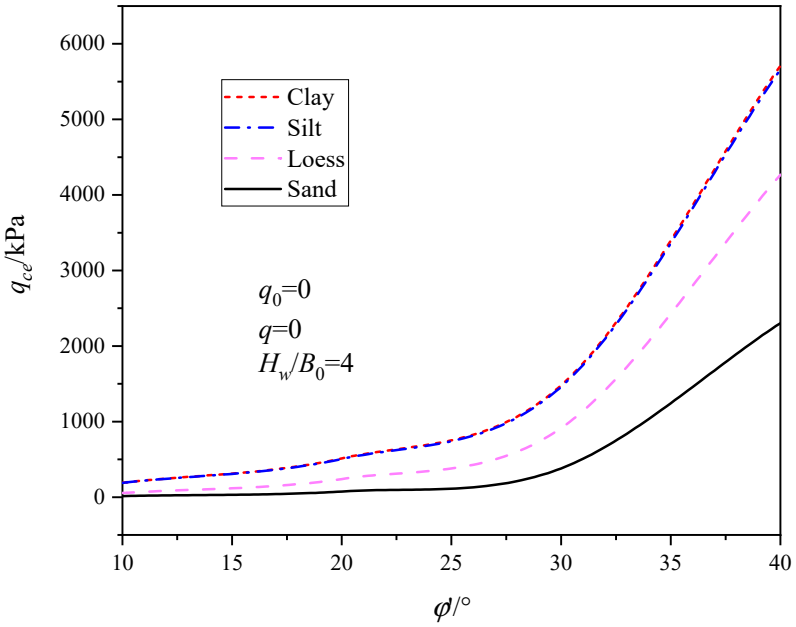

Figure 14. The optimal bearing capacity q_{ce} varies with φ' for four types of soils.

Figure 15 depicts the variation of the q_{ce} with the uniform load q_0 for four unsaturated soils. The values of the other parameters are labeled in the figure. For all four unsaturated soils, the same trend is demonstrated, with the optimal bearing capacity q_{ce} increasing with q_0. For the sand, the optimal bearing capacity q_{ce} at $q_0 = 30$ kPa is 236% higher than that at $q_0 = 0$ kPa. Therefore, the uniform load q_0 has an important influence on the q_{ce} of reinforced strip footings on unsaturated soils, and the q_{ce} can be improved by increasing the uniform load q_0.

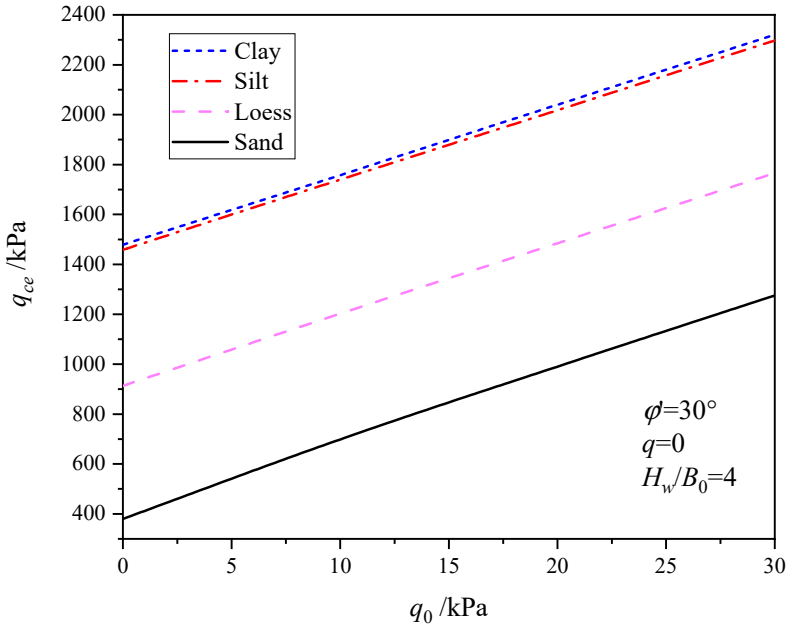

Figure 15. The optimal bearing capacity q_{ce} varies with uniform load q_0 for four types of soils.

5.3. Effect of Steady Flow

The purpose of this subsection is to discuss the influence of steady flow effects on the optimal bearing capacity of reinforced foundations. There are a total of four parameters that characterize the properties of unsaturated soils, including the flow rate q, the hydraulic

conductivity k_s, and the fitting parameters α and ψ. In addition to the above parameters, the water table H_w is also an important index.

Figure 16 illustrates the change of the optimal bearing capacity q_{ce} with H_w/B_0 for four unsaturated soils at different q. In addition, the q_{ce} of the unreinforced case and the reinforced case for different parameter values are compared. For both clay and silt, the optimal bearing capacity q_{ce} increases with increasing H_w/B_0, however, the former grows linearly and the latter non-linearly. Due to the difference in apparent cohesion, the trend of the q_{ce} of foundations on loess or sand is different from the above. For the loess, the optimal bearing capacity q_{ce} increases and then decreases with increasing H_w/B_0, reaching a peak at $H_w/B_0 = 4$. For the sand, the optimal bearing capacity q_{ce} decreases as H_w/B_0 increases, and q_{ce} decreases more slowly when H_w/B_0 is greater than four. Therefore, for different unsaturated soils, pay close attention to the effects of the water table depth H_w.

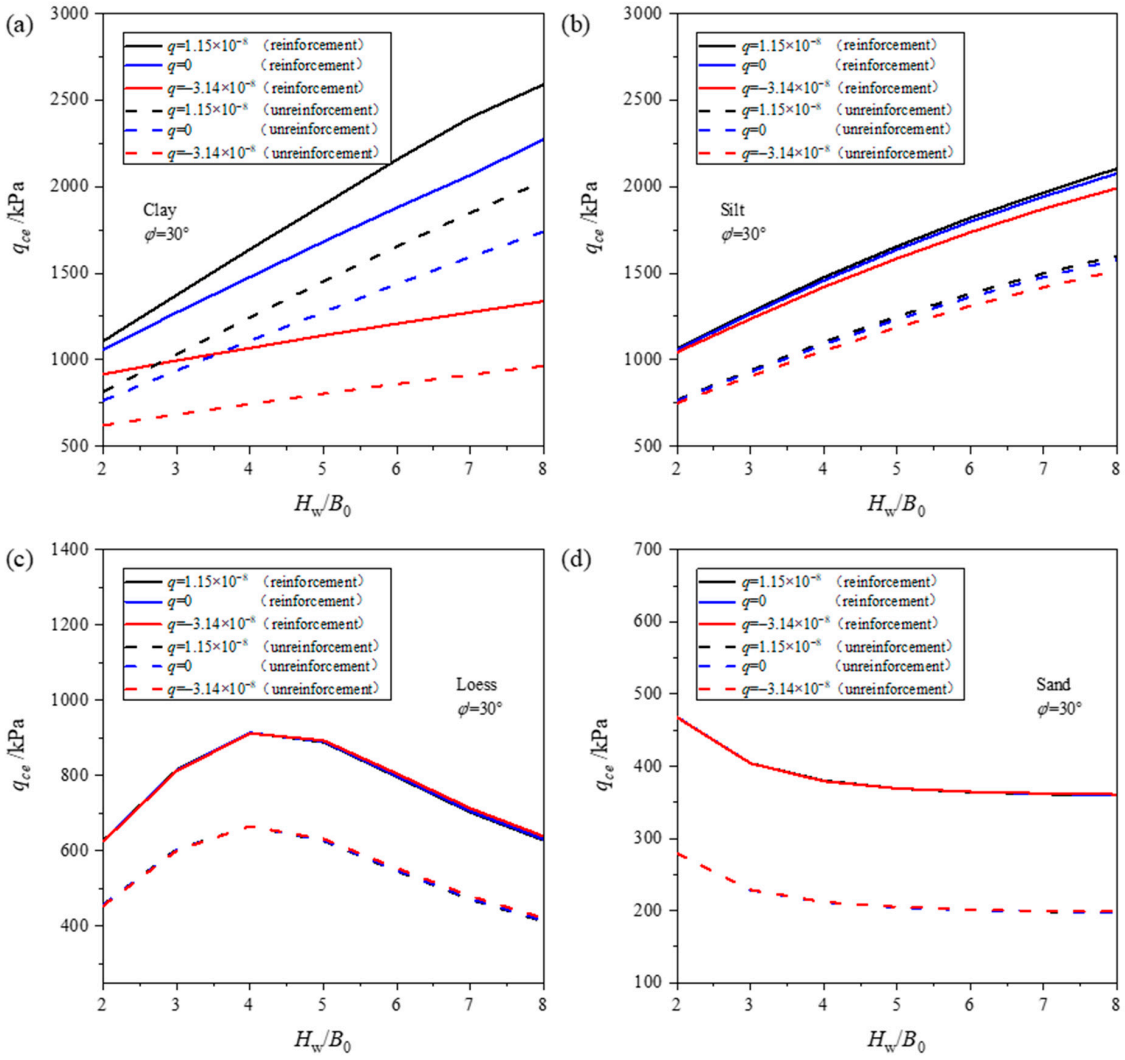

Figure 16. Variation of the optimal bearing capacity q_{ce} with H_w/B_0 for different q under reinforced or unreinforced conditions. (**a**) Clay, (**b**) Silt, (**c**) Loess, (**d**) Sand.

In order to better visualize the pattern of the obtained results, the percentage increase in bearing capacity is given. For example, for clay, when H_w/B_0 increases from 2 to 8, the optimal bearing capacity increases by about 114% at $q = 0$. For silt, the optimal bearing capacity increases by about 96%. For loess, the optimal bearing capacity at $H_w/B_0 = 4$ is about 45% higher than that at $H_w/B_0 = 2$. However, for sand, the optimal bearing capacity decreases by about 23% when H_w/B_0 goes from 2 to 8. The above data shows that for

different types of unsaturated soils, the effect of H_w/B_0 on bearing capacity is different; therefore, targeted design is needed in actual engineering.

From Figure 16, the flow rate q also influences the optimal bearing capacity, especially for strip footings on clay. For loess and sand, the influence of the flow rate q on the optimal bearing capacity is weak. The overall order of magnitude of bearing capacity is evaporative conditions > no-flow conditions > infiltration conditions. Compared to the unreinforced condition, the q_{ce} of the reinforced strip footings on unsaturated soils is significantly improved. The optimal bearing capacity curve for the reinforced case follows the same trend as that for the unreinforced case. In addition, it can be found that when $q = 0$ and $H_w/B_0 = 2$, the optimal bearing capacity is increased by about 38% for all the first three unsaturated soils compared to the unreinforced case (clay, silt, and loess), while for sand, the bearing capacity is increased by about 67%. Therefore, the poorer the soil quality, the greater the enhancement of the bearing capacity of foundations by reinforcement measures.

For the case of $B_0 = 1$ m, $\varphi' = 30°$, $c' = 10$ kPa, $q_0 = 0$ kPa, $k_s = 5 \times 10^{-8}$ m/s, and $q = 0$ m/s, Figure 17 gives the trend of the optimal bearing capacity q_{ce} with $1/\alpha$ at different ψ and H_w/B_0. When ψ is constant, the optimal bearing capacity q_{ce} increases with $1/\alpha$. While for a definite value of $1/\alpha$, the optimal bearing capacity q_{ce} decreases with increasing ψ. For different ψ, except for $\psi = 1.1$, the larger ψ is, the slower the optimal bearing capacity curve rises. However, for $\psi = 1.1$, the trend of the optimal bearing capacity q_{ce} is similar for different H_w/B_0, which is slowly increasing.

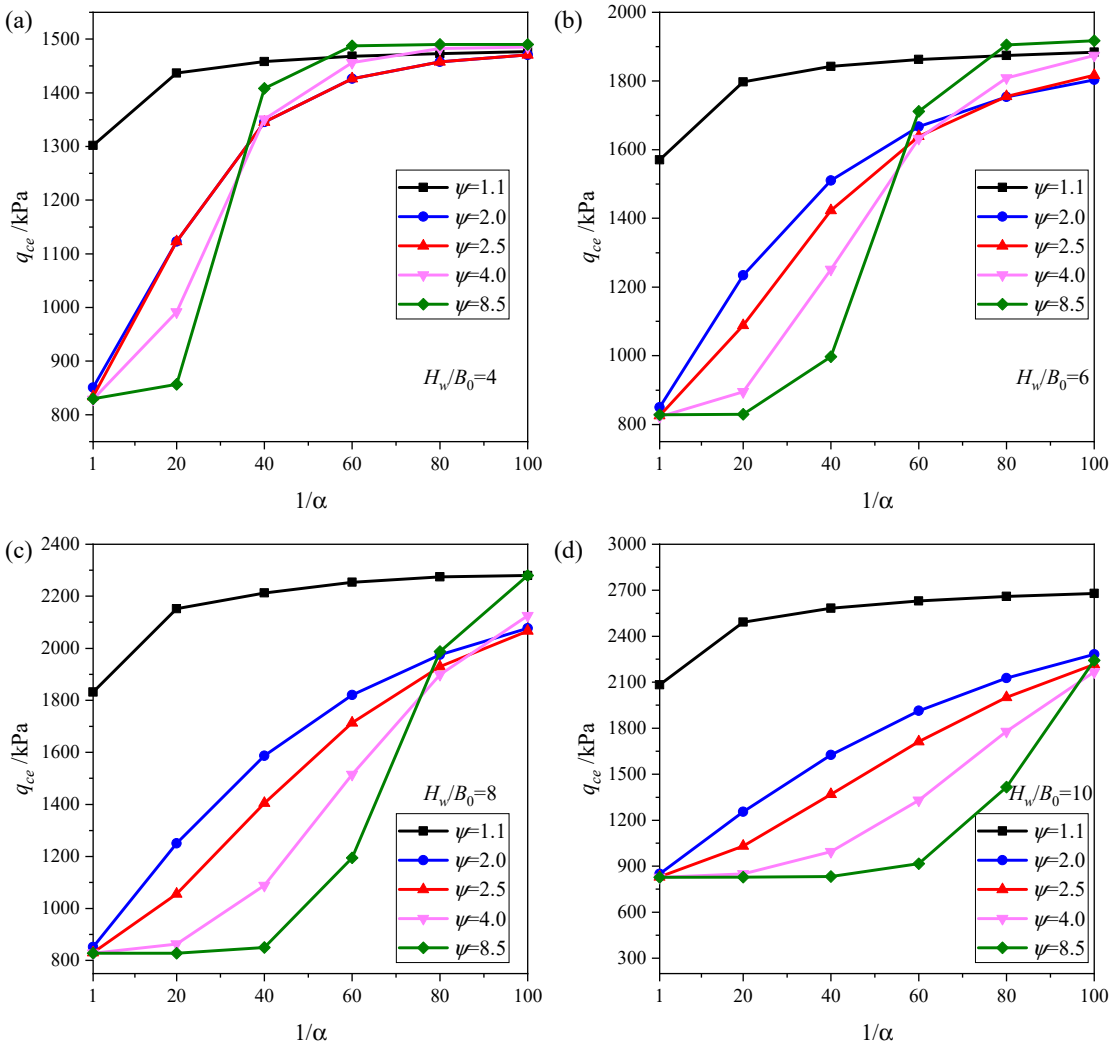

Figure 17. Variation of the optimal bearing capacity q_{ce} with $1/\alpha$ at different ψ in case of (**a**) $H_w/B_0 = 4$, (**b**) $H_w/B_0 = 6$, (**c**) $H_w/B_0 = 8$, (**d**) $H_w/B_0 = 10$.

When $H_w/B_0 = 4$, as $1/\alpha$ increases from 1 to 100, the optimal bearing capacity increases by about 13%, 72%, 76%, 79%, and 80% for $\psi = 1.1$, ψ= 2.0, ψ= 2.5, ψ= 4.0 and ψ= 8.5, respectively. It can be found that the percentage increase in the optimal bearing capacity tends to a certain range as ψ increases. When $1/\alpha = 1$, the optimal bearing capacity at $\psi = 1.1$ is significantly larger than the result when ψ takes any other value, where the maximum difference occurs at $H_w/B_0 = 10$. In addition, when $1/\alpha = 1$, the optimal bearing capacity increases continuously as H_w/B_0 increases in the case of $\psi = 1.1$, however, for the other four cases (ψ= 2.0, 2.5, 4.0, 8.5), the optimal bearing capacity remains almost constant. However, as $1/\alpha$ increases, the above situation improves.

From Figure 17, all the curves converge to a certain range as $1/\alpha$ increases, and the convergence of the curve becomes slower as H_w/B_0 increases. However, the location of the inflection point of the optimal bearing capacity curve is gradually shifted to the right with the increase of H_w/B_0. In addition, it is to be noted that as H_w/B_0 increases, the value of the q_{ce} for the final convergence also increases. Therefore, deep water table H_w contribute to the q_{ce} of reinforced footings on unsaturated soils. Through the above analysis, it can be known that H_w/B_0, $1/\alpha$, ψ all have significant influence on the optimal bearing capacity of reinforced soil foundations, and the values of each parameter should be accurately selected according to the actual situation during design.

6. Conclusions

In this paper, the analytical solution for the bearing capacity of reinforced strip footings on unsaturated soils is obtained for the first time. Considering the effect of matrix suction, the apparent cohesion at different depths is calculated using Lu et al.'s suction stress formula, thus reflecting the properties of unsaturated soils. Depending on the relative position of the reinforcement and the slide surface, two failure mechanisms are constructed. Based on the upper bound theorem of limit analysis and considering the work conducted by the reinforcement, the bearing capacity formulas under the above two failure mechanisms are derived, respectively. Each formula includes $2n + 1$ variables, which are optimized by adopting the SQP algorithm to obtain an upper bound solution. Then, compare the results of the two failure mechanisms to find the optimal bearing capacity of the reinforced footing on unsaturated soils. The validity of the methodology of this paper is verified by comparing the results with those of other literature.

To investigate the influence of one-dimensional steady flow on the bearing capacity of reinforced soil foundations, four typical soils are selected for parametric analysis in this paper. The research results enhance understanding of reinforced strip foundations on unsaturated soils, and the work outcomes provided the following results:

(1) Considering both the effect of reinforcement as well as the effect of matrix suction, analytical expressions for the bearing capacity of reinforced strip footings on unsaturated soils are given in this paper, and results are obtained for four typical unsaturated soils. In addition, the expressions apply to any unsaturated soil for which the relevant parameters can be given.

(2) The bearing capacity increases and then decreases with d/B_0. In this paper, for four types of soils, the range of reinforcement embedment depth at 50% of the maximum increase in bearing capacity is given, as shown in Figure 12, which can be used in engineering practice.

(3) The optimal bearing capacity q_{ce} increases with a uniform load q_0. For sand, the optimal bearing capacity is increased by about 236% when q_0 is increased from 0 to 30 kPa. For loess, the optimal bearing capacity is increased by about 93%. And because the clay is similar to the silt, the optimal bearing capacity is increased by about 57%.

(4) For all four types of soils, the optimal bearing capacity q_{ce} increases with the effective internal friction angle φ'. In addition, the effective internal friction angle φ' significantly affects the optimal embedment depth d of the reinforcement as well as the optimal bearing capacity ratio q_{ce}/q_{ce0}.

(5) Compared to the no-flow case ($q = 0$ m/s), the evaporation case ($q > 0$ m/s) increases the optimal bearing capacity and the infiltration case ($q < 0$ m/s) decreases the optimal bearing capacity. The order of degree of influence of flow rate q on the four unsaturated soils is as follows: Clay > Silt > Loess > Sand. In addition, for the clay, the optimal d/B_0 increases as the flow rate q increases.

(6) For clay and silt, the optimal bearing capacity q_{ce} increases with an increasing water table H_w. On the contrary, for the sand, the optimal q_{ce} decreases with increasing H_w. However, for the loess, the optimal q_{ce} increases and then decreases, and the optimal bearing capacity is maximized when $H_w/B_0 = 4$.

(7) For different values of ψ, the q_{ce} increases with $1/\alpha$ and eventually converges to a certain range. In addition, the larger ψ is, the more slowly the optimal bearing capacity curve rises. For example, when $H_w/B_0 = 4$ and $\psi = 8.5$, the optimal bearing capacity increases by about 80% when $1/\alpha$ goes from 1 to 100.

This paper gives a theoretical basis for the calculation of the bearing capacity of reinforced strip footings on unsaturated soils; however, there are some limitations. The paper assumes that the strength of the reinforcement is adequate and mainly investigates the sliding failure mode without considering the effect of reinforcement rupture. This direction should be explored in future work. In future work, some mathematical modeling and optimization methods should also be used to deal with the data [45,46], which will lead to a deeper understanding of the intrinsic connection between variables and results. In addition, the work can be further extended by, for example, considering seismic effects, layered soils, nonlinear failure criteria of soils, and transient flow.

Author Contributions: Methodology, X.K.; Validation, D.Z.; Data curation, X.K.; Writing—original draft, X.K.; Supervision, D.Z. All authors have read and agreed to the published version of the manuscript.

Funding: This research received no external funding.

Data Availability Statement: Data supporting the reported results can be provided by the corresponding author at reasonable request.

Conflicts of Interest: The authors declare no conflict of interest.

Appendix A

$$f_1 = \frac{\cos\varphi' \cos(\beta_1 - \theta - \varphi')}{2\cos\theta \sin(\beta_1 - 2\varphi')}$$

$$f_2 = \frac{\cos\varphi' \cos(\theta - \varphi')}{2\cos\theta \sin(\beta_1 - 2\varphi')} \cdot \sum_{i=2}^{n} \left[\frac{\sin(\beta_{i-1} - \beta_i + \alpha_{i-1})}{\sin(\beta_1 - 2\varphi')} \cdot \prod_{j=1}^{i-1} \frac{\sin\beta_j}{\sin(\alpha_j + \beta_j)} \cdot \prod_{j=1}^{i-2} \frac{\sin(\alpha_j + \beta_j - 2\varphi')}{\sin(\beta_{j+1} - 2\varphi')} \right]$$

$$f_3 = \frac{\cos\varphi' \cos(\theta - \varphi')}{2\cos\theta \sin(\beta_1 - 2\varphi')} \cdot \sum_{i=1}^{n} \left[\frac{\sin\alpha_i}{\sin(\alpha_i + \beta_i)} \cdot \prod_{j=1}^{i-1} \frac{\sin\beta_j \sin(\alpha_j + \beta_j - 2\varphi')}{\sin(\alpha_j + \beta_j) \sin(\beta_{j+1} - 2\varphi')} \right]$$

$$f_4 = \frac{\tan\theta}{2}$$

$$f_5 = \frac{\cos(\theta - \varphi')}{2\cos^2\theta \sin(\beta_1 - 2\varphi')} \cdot \sum_{i=1}^{n} \left[\frac{\sin\alpha_i \sin\beta_i}{\sin(\alpha_i + \beta_i)} \sin\left(\beta_i - \theta - \varphi' - \sum_{j=1}^{i-1} \alpha_j \right) \cdot \prod_{j=1}^{i-1} \frac{\sin^2\beta_j \sin(\alpha_j + \beta_j - 2\varphi')}{\sin^2(\alpha_j + \beta_j) \sin(\beta_{j+1} - 2\varphi')} \right]$$

$$f_6 = \frac{\cos(\theta-\varphi')}{\cos\theta\sin(\beta_1-2\varphi')}\frac{\sin\beta_n}{\sin(\alpha_n+\beta_n)}\sin\left(\beta_n-\theta-\varphi'-\sum_{j=1}^{n-1}\alpha_j\right)\cdot\prod_{j=1}^{n-1}\frac{\sin\beta_j\sin(\alpha_j+\beta_j-2\varphi')}{\sin(\alpha_j+\beta_j)\sin(\beta_{j+1}-2\varphi')}$$

Effective embedded length of reinforcement $l_{e,i}$:

$$l_{e,i} = d\left(\cot\left(\theta+\sum_{1}^{i-1}\alpha_i\right)-\cot\left(\theta+\sum_{1}^{i}\alpha_i\right)\right) \qquad 1\le i\le n-1$$

$$l_{e,n}= \min\left\{B(n)\frac{\sin\beta_n}{\sin(\alpha_n+\beta_n)}-d(\cot\alpha_n-\cot(\alpha_n+\beta_n)),\qquad 1.5B_0-d\cot(\alpha_n)\right\} \qquad i=n$$

Constraints:

$$0<\alpha_i<\pi/2$$
$$0<\beta_i<\pi$$
$$\alpha_i+\beta_i\ge\beta_{i+1}$$
$$\theta+\alpha_1+\alpha_2+\cdots+\alpha_n=\pi$$
$$h_{\max}\le d(\mathrm{M2})$$

where $h_{\max}$ means the maximum depth of the failure mechanism (M2).

References

1. Michalowski, R.L. Limit loads on reinforced foundation soils. *J. Geotech. Geoenviron. Eng.* **2004**, *130*, 381–390. [CrossRef]
2. Manna, D.; Santhoshkumar, G.; Ghosh, P. Upper-bound limit load of rigid pavements resting on reinforced soil embankments–Kinematic approach. *Transp. Geotech.* **2021**, *30*, 100611. [CrossRef]
3. Rezai Soufi, G.; Jamshidi Chenari, R.; Bathurst, R.J. Seismic bearing capacity of geosynthetic reinforced strip footings using upper bound limit analysis. *Int. J. Geomech.* **2022**, *22*, 04021300. [CrossRef]
4. Yang, X.L.; Yin, J.H. Upper bound solution for ultimate bearing capacity with a modified Hoek-Brown failure criterion. *Int. J. Rock Mech. Min. Sci.* **2005**, *42*, 550–560. [CrossRef]
5. Liu, J.; Xu, S.; Yang, X.L. Modified pseudo–dynamic bearing capacity of strip footing on rock masses. *Comput. Geotech.* **2022**, *150*, 104897. [CrossRef]
6. Loret, B.; Khalili, N. A three-phase model for unsaturated soils. *Int. J. Numer. Anal. Meth. Geomech.* **2000**, *24*, 893–927. [CrossRef]
7. Vanapalli, S.K.; Mohamed, F.M.O. Bearing capacity and settlement of footings in unsaturated sands. *Int. J. Geomech.* **2013**, *5*, 595–604. [CrossRef]
8. Binquet, J.; Lee, K.L. Bearing capacity tests on reinforced earth slabs. *J. Geotech. Eng. Div.* **1975**, *101*, 1241–1255. [CrossRef]
9. Huang, C.C.; Tatsuoka, F. Bearing capacity of reinforced horizontal sandy ground. *Geotext. Geomembr.* **1990**, *9*, 51–82. [CrossRef]
10. Das, B.M.; Shin, E.C.; Omar, M.T. The bearing capacity of surface strip foundations on geogrid-reinforced sand and clay—A comparative study. *Geotech. Geol. Eng.* **1994**, *12*, 1–14. [CrossRef]
11. Raja, M.N.A.; Shukla, S.K. Experimental study on repeatedly loaded foundation soil strengthened by wraparound geosynthetic reinforcement technique. *J. Rock Mech. Geotech. Eng.* **2021**, *13*, 899–911. [CrossRef]
12. Chen, Q.; Abu-Farsakh, M.; Sharma, R.; Zhang, X. Laboratory investigation of behavior of foundations on geosynthetic-reinforced clayey soil. *Transp. Res. Rec. J. Transp. Res. Board* **2007**, *2004*, 28–38. [CrossRef]
13. Ghazavi, M.; Lavasan, A.A. Interference effect of shallow foundations constructed on sand reinforced with geosynthetics. *Geotext. Geomembr.* **2008**, *26*, 404–415. [CrossRef]
14. Binquet, J.; Lee, K.L. Bearing capacity analysis of reinforced earth slabs. *J. Geotech. Eng. Div.* **1975**, *101*, 1257–1276. [CrossRef]
15. Kumar, A.; Saran, S. Bearing capacity of rectangular footing on reinforced soil. *Geotech. Geol. Eng.* **2003**, *21*, 201–224. [CrossRef]
16. Yamamoto, K.; Otani, J. Bearing capacity and failure mechanism of reinforced foundations based on rigid-plastic finite element formulation. *Geotext. Geomembr.* **2002**, *20*, 367–393. [CrossRef]
17. Maharaj, D.K. Nonlinear finite element analysis of strip footing on reinforced clay. *Electron. J. Geotech. Eng.* **2003**, *8*, 241–256.
18. Izadi, A.; Nalkiashari, L.A.; Payan, M.; Chenari, R.J. Bearing capacity of shallow strip foundations on reinforced soil subjected to combined loading using upper bound theorem of finite element limit analysis and second-order cone programming. *Comput. Geotech.* **2023**, *160*, 105550. [CrossRef]
19. Wang, Z.J.; Jacobs, F.; Ziegler, M.; Yang, G.Q. Visualisation and quantification of geogrid reinforcing effects under strip footing loads using discrete element method. *Geotext. Geomembr.* **2020**, *48*, 62–70. [CrossRef]
20. Chen, J.F.; Bao, N.; Sun, R. Three-dimensional discrete-element-method analysis of behavior of geogrid-reinforced sand foundations under strip footing. *Int. J. Geomech.* **2022**, *22*, 04022134. [CrossRef]

21. Nazeeh, K.M.; Sivakumar Babu, G.L. Reliability-based design of geogrid reinforced soil foundation using kriging surrogates. *Geosynth. Int.* **2022**, *30*, 350–363. [CrossRef]
22. Banović, I.; Radnić, J.; Grgić, N. Geotechnical seismic isolation system based on sliding mechanism using stone pebble layer: Shake-table experiments. *Shock. Vib.* **2019**, *2019*, 9346232. [CrossRef]
23. Su, L.; Lu, J.; Elgamal, A.; Arulmoli, A.K. Seismic performance of a pile-supported wharf: Three-dimensional finite element simulation. *Soil Dyn. Earthq. Eng.* **2017**, *95*, 167–179.
24. Forcellini, D.; Alzabeebee, S. Seismic fragility assessment of geotechnical seismic isolation (GSI) for bridge configuration. *Bull. Earthq. Eng.* **2023**, *21*, 3969–3990. [CrossRef]
25. Mortazavi Bak, H.; Noorbakhsh, M.; Halabian, A.M.; Rowshanzamir, M.; Hashemolhosseini, H. Application of the Taguchi method to enhance bearing capacity in geotechnical engineering: Case studies. *Int. J. Geomech.* **2021**, *21*, 04021167. [CrossRef]
26. Zhang, L.L.; Fredlund, D.G.; Fredlund, M.D.; Wilson, G.W. Modeling the unsaturated soil zone in slope stability analysis. *Can. Geotech. J.* **2014**, *51*, 1384–1398. [CrossRef]
27. Fredlund, D.G.; Morgenstern, N.R.; Widger, R.A. The shear strength of unsaturated soils. *Can. Geotech. J.* **1978**, *15*, 313–321. [CrossRef]
28. Oloo, S.Y.; Fredlund, D.G.; Gan, J.K.M. Bearing capacity of unpaved roads. *Can. Geotech. J.* **1997**, *34*, 398–407. [CrossRef]
29. Costa, Y.D.; Cintra, J.C.; Zornberg, J.C. Influence of matric suction on the results of plate load tests performed on a lateritic soil deposit. *Can. Geotech. J.* **2003**, *2*, 219–226.
30. Vanapalli, S.K.; Mohamed, F.M.O. Bearing capacity of model footings in unsaturated soils. In *Experimental Unsaturated Soil Mechanics*; Schanz, T., Ed.; Springer: Berlin/Heidelberg, Germany, 2007; pp. 483–493.
31. Oh, W.T.; Vanapalli, S.K. Modelling the applied vertical stress and settlement relationship of shallow foundations in saturated and unsaturated sands. *Can. Geotech. J.* **2011**, *48*, 425–438. [CrossRef]
32. Lu, N.; Likos, W.J. Suction stress characteristic curve for unsaturated soil. *J. Geotech. Geoenviron. Eng.* **2006**, *132*, 131–142.
33. Lu, N.; Godt, J.W.; Wu, D.T. A closed-form equation for effective stress in unsaturated soil. *Water Resour. Res.* **2010**, *46*, 8646.
34. Vahedifard, F.; Robinson, J.D. Unified Method for Estimating the Ultimate Bearing Capacity of Shallow Foundations in Variably Saturated Soils under Steady Flow. *J. Geotech. Geoenviron. Eng.* **2016**, *142*, 1445.
35. Du, D.; Zhuang, Y.; Sun, Q.; Yang, X.; Dias, D. Bearing capacity evaluation for shallow foundations on unsaturated soils using discretization technique. *Comput. Geotech.* **2021**, *137*, 104309.
36. Xu, S.; Zhou, D. Seismic Bearing Capacity Solution for Strip Footings in Unsaturated Soils with Modified Pseudo-Dynamic Approach. *Mathematics* **2023**, *11*, 2692.
37. Yang, X.L.; Huang, F. Collapse mechanism of shallow tunnel based on nonlinear Hoek–Brown failure criterion. *Tunn. Undergr. Space Technol.* **2011**, *26*, 686–691. [CrossRef]
38. Yang, X.L.; Li, L.; Yin, J.H. Seismic and static stability analysis for rock slopes by a kinematical approach. *Geotechnique* **2004**, *54*, 543–549.
39. Yang, X.L.; Wang, J.M. Ground movement prediction for tunnels using simplified procedure. *Tunn. Undergr. Space Technol.* **2011**, *26*, 462–471.
40. Hou, C.T.; Zhong, J.H.; Yang, X.L. Three-dimensional stability assessments of a non-circular tunnel face reinforced by bolts under seepage flow conditions. *Tunn. Undergr. Space Technol.* **2023**, *131*, 104831.
41. Hu, Y.N.; Ji, J.; Sun, Z.B.; Dias, D. First order reliability-based design optimization of 3D pile-reinforced slopes with Pareto optimality. *Comput. Geotech.* **2023**, *162*, 105635.
42. Gardner, W.R. Some steady-state solutions of the unsaturated moisture flow equation with application to evaporation from a water table. *Soil Sci.* **1958**, *85*, 228–232.
43. Soubra, A. Upper-bound solutions for bearing capacity of foundations. *J. Geotech. Geoenviron. Eng.* **1999**, *125*, 59–68.
44. Kumar, J.; Sahoo, J.P. Bearing capacity of strip foundations reinforced with geogrid sheets by using upper bound finite-element limit analysis. *Int. J. Numer. Anal. Methods Geomech.* **2013**, *37*, 3258–3277.
45. Kondrakhin, V.P.; Martyushev, N.V.; Klyuev, R.V.; Sorokova, S.N.; Efremenkov, E.A.; Valuev, D.V.; Mengxu, Q. Mathematical Modeling and Multi-Criteria Optimization of Design Parameters for the Gyratory Crusher. *Mathematics* **2023**, *11*, 2345.
46. Negrin, I.; Kripka, M.; Yepes, V. Metamodel-assisted meta-heuristic design optimization of reinforced concrete frame structures considering soil-structure interaction. *Eng. Struct.* **2023**, *293*, 116657.